PCCP

Accepted Manuscript

ROYAL SOCIETY OF CHEMISTRY

www.rsc.org/pccp

Cite this: DOI: 10.1039/c0xx00000x

www.rsc.org/xxxxxx

ARTICLE TYPE

The role of the oleic acid on the synthesis of $Fe_{3-x}O_4$ nanoparticles over a wide size range

Carlos Moya,* Xavier Batlle, Amílcar Labarta

Received (in XXX, XXX) Xth XXXXXXXXX 20XX, Accepted Xth XXXXXXXXX 20XX
DOI: 10.1039/b000000x

This work reports on the role of the oleic acid concentration on the magnetic and structural properties of $Fe_{3-x}O_4$ nanoparticles synthesized by thermal decomposition of $Fe(acac)_3$ in benzyl-ether. This method allows the synthesis of highly monodisperse particles ranging from 7 to 100 nm in size by only varying the concentration of the oleic acid in the reaction mixture. The structural and magnetic characterizations reveal homogeneous particles in composition, with narrow particle size distribution, which are single-phase magnetite with almost bulk-like values of the saturation magnetization of about 90-99 emu/g at low temperatures and showing the characteristic anomaly in the zero field-cooling magnetization curves associated with the Verwey transition for nanoparticles bigger than about 7 nm. In addition, the analyses of aliquots of the reaction mixtures by Fourier transform infrared spectroscopy at various stages shed light about the nucleation and growing processes of the particles.

Introduction

$Fe_{3-x}O_4$ nanoparticles (NPs) have been widely investigated because of their high value of the saturation magnetization at room temperature, low-toxicity, easy functionalization and fast response to an external magnetic field.[1,2] Those properties make them excellent candidates for potential applications in technology and biomedicine[3], such as catalysis,[4] hyperthermia,[5,6] drug delivery,[7] NMR contrast agents or data storage.[8-10] Besides and from the fundamental point of view,[11] those NPs are ideal system models to study the new magnetic phenomenology associated with the so-called *particle-like* behaviour, which emerges from the size reduction towards the nanometer scale and contrasts with the well-established magnetic properties of their bulk-counterparts. It has been shown that most of the particle-like behaviour and in general the large variability of the magnetic properties observed in this kind of nanomaterials are related to structural features of the NPs rather than being originated from intrinsic finite-size or surface effects, at least for NPs bigger than a few nanometers.[12-15] These structural features, such as crystallographic defects, polycrystalline nature of the NPs, lack of crystallinity at the particle surface, etc., have strong influence on their magnetic properties and can be modified at will through the synthesis method. So that, whenever this particle-like behaviour is unwanted for specifics applications, the choice of a suitable synthesis method is of key importance to obtain nanoparticles of high-crystalline quality.[16] The thermal decomposition of an organic precursor stands up among those methods used to obtain $Fe_{3-x}O_4$ NPs, since it yields monodisperse NPs with excellent magneto-structural properties, such as single-phase NPs which are crystalline monodomains and exhibit high values of the saturation magnetization very close to that of the bulk material.[17-19] Typically, in this method, either decanoic or oleic acids and oleylamine are used as surfactants that react with the metallic organic precursor to form an intermediate Fe^{3+}-complex that in turn decomposes to form $Fe_{3-x}O_4$,[20,21] together with 1,2-hexadecanediol as stabilizer agent and several organic solvents with high boiling points as reaction medium.[14,22] However and although all the chemicals needed for the reaction are well-established, some drawbacks and lack of reproducibility are observed when trying to scale up the method due to the great number of reactants involved, fact that complicates a proper characterization of the reaction mechanisms. In this sense, we reported on the synthesis of iron oxide NPs in a wide size range from a reaction mixture containing only decanoic acid and iron acetylacetonate.[23, 24]

Within this framework, we present a systematic study where we control the size of the obtained $Fe_{3-x}O_4$ NPs from about 7 to 100 nm by only varying the amount of oleic acid in the reaction mixture, using in all the cases benzyl-ether as the carrier solvent. In addition, we show that the samples exhibit excellent magnetic properties very close to those of bulk magnetite. To gain a deeper insight into the reaction mechanisms some aliquots of the reaction mixture at several stages were studied by Fourier transform infrared (FTIR) spectroscopy. The results show that the iron acetylacetonate totally decomposes at 200 ºC to form an intermediate metal-complex, no matter the amount of oleic acid present in the reaction. Therefore, we demonstrate that the nucleation and growth processes of the NPs caused by the further decomposition of the intermediate metal-complex can be controlled by means of solely the concentration of oleic acid.

Experimental Section

Sample preparation

Five samples of $Fe_{3-x}O_4$ NPs were synthesized in order to study the effect of the oleic acid concentration on particle size and magneto-structural properties, by using iron (III) acetylacetonate (Sigma-Aldrich, 99%) as precursor, and oleic acid (Sigma-Aldrich 90) and benzyl-ether (Sigma-Aldrich, 98%) as surfactant and organic solvent, respectively. All the reactants were used in the synthesis without further purification.

Sample R1. 0.36 g of $Fe(acac)_3$ (1 mmol) and 1.73 g of oleic acid (6 mmol) were mixed in 25 mL of benzyl-ether. The reaction mixture was degassed at 60 ºC for 30 min, then, heated up to 200 ºC, and kept at this temperature for 2 h under a nitrogen atmosphere and vigorous stirring. After that, the solution was heated up at 5 ºC/min to reflux temperature (270 ºC) and kept at this temperature for 1 h. After cooling down to room temperature, a mixture of ethanol and 1-propanol with the volume ratio 3:1 was added to the solution. Then, the mixture was centrifuged to precipitate the NPs. The precipitate was decanted, washed several times and finally redispersed in hexane.

Samples R2-R5. Bigger NPs were obtained following the former procedure but reducing the concentration of oleic acid in the reaction mixture as follows: **R2** (1,15 g, 4 mmol), **R3** (0.87g, 3 mmol) **R4** (0.58 g, 2 mmol) and **R5** (without using oleic acid in the reaction mixture). The precipitate for samples **R2-R5** was redispersed in ethanol.

Experimental techniques

The shape and size of the NPs were determined by transmission electron microscopy (TEM) using a MT80-Hitachi microscope. To prepare the samples for TEM experiments, one drop of a dilute suspension of NPs in an appropriate solvent was placed onto a carbon-coated cooper grid and dried at room temperature. The size distributions were obtained by measuring at least 1500 particles and the resultant histograms were fitted to log-normal functions (see Fig. S1 for samples R1, R2, R3 and R4 and Fig. S3d for R5, Supporting information). The mean particle size (D_{TEM}) and the unitless standard deviation of the log-normal distribution (σ) were obtained from these fits (see Table 1). In order to get insight about the crystal quality of the samples, high resolution transmission microscopy (HRTEM) was carried out by using JEOL-2100 microscope (see Fig. 1e-h and Fig. S2 and S3b-c, Supporting information).

The crystallographic structure of the particles was identified by X-ray powder diffraction (XRD) performed in a PANalytical X'Pert PRO MPD diffractometer by using Cu Kα radiation. The patterns were collected within 5 and 120º in 2θ. In all cases, the XRD spectra were indexed to an inverse spinel structure (see Fig. 3). The mean size of the crystal domains (D_{XRD}) obtained from XRD spectra are given in Table 1.

The organic fraction of the samples was evaluated by thermogravimetric analysis (TGA). Measurements were performed in a TGA-SDTA 851e/SF/1100 (Mettler Toledo) at a heating rate of 10 ºC min^{-1} in nitrogen atmosphere from room temperature up to 800 ºC (see Fig. S4, Supporting information).

2 mL aliquots of the reaction mixtures collected at several stages along the reactions to synthesize R1-R5 samples were studied by means of Fourier transform infrared (FTIR) spectroscopy (see Fig. 7 and Fig. S6, Supporting information) with a Thermo SCIENTIFIC NICOLET iZ10 in the energy range between 4000 and 400 cm^{-1} with a spectral resolution of 4 cm^{-1}.

Magnetization measurements in powder samples were performed with a Quantum Design SQUID magnetometer. Hysteresis loops, $M(H)$, were recorded at several temperatures within 5 and 300 K under a maximum magnetic field of ± 50 kOe to study the saturation magnetization M_s and coercive field H_c (see Fig. 4 and S5a, Supporting information). M_s was obtained by extrapolation of the high-field region of $M(H)$ to zero field, assuming the high-field behaviour $M(H) = M_s + \chi \cdot H$, where χ is a residual susceptibility (see Table 1). M_s values were normalized to the magnetic content by subtracting the organic fraction determined by TGA measurements. H_c was defined as $H_c = (|H_c^+| + |H_c^-|)/2$. In order to investigate the presence of various magnetic phases, hysteresis loops were recorded after field cooling the sample from 300 K down to the final measuring temperature under an applied magnetic field of 10 kOe (see Fig. 5 and S5a, Supporting information). The thermal dependence of the magnetization was studied after zero field cooling (M_{ZFC}) and field cooling (M_{FC}) the samples. These curves were collected using the following protocol. The sample was cooled down from 300 to 2 K in zero magnetic field. Then, a static magnetic field of 50 Oe was applied and M_{ZFC} was measured while warming up from 2 to 300 K. Once room temperature was reached, the sample was cooled down again to 2 K while 50 Oe was applied. Finally, the sample was rewarmed up to 300 K and M_{FC} was collected under an applied field of 50 Oe (see Fig. 6 and S5b, Supporting information).

Results and discussion

Structural characterization

TEM images for samples R1-R4 show particles with narrow size distributions (see Table 1 and Fig. S1, Supporting information) and distinct shapes depending on the NP size, that go from pseudo-spherical NPs for R1 to faceted ones for R2-R4 (see Fig. 1a-d). In addition, micrograph images for R1 and R2, those samples with the smallest particles, reveal the formation of self-assemblies in a hexagonal close-packing arrangement of the NPs as a consequence of their monodispersity, shape regularity and the fact that the particles are smaller than about 20 nm in both samples. Besides, HRTEM images show certain degradation on the crystalline quality of the NPs as their size is increased (see Fig. 1e-h). In contrast to the good crystallinity observed in the HRTEM images for samples R1 and R2, samples R3 and R4 show particles with some crystalline defects and irregularities that could be attributed to faster particle growing during the synthesis (see Fig. S2, Supporting information). From these results, it can be concluded the key role of the oleic acid concentration on the reaction mixture to tune the mean particle size, as it is shown in Fig. 2 where an abrupt increase on the average size of the particles is observed as the oleic acid concentration is reduced.

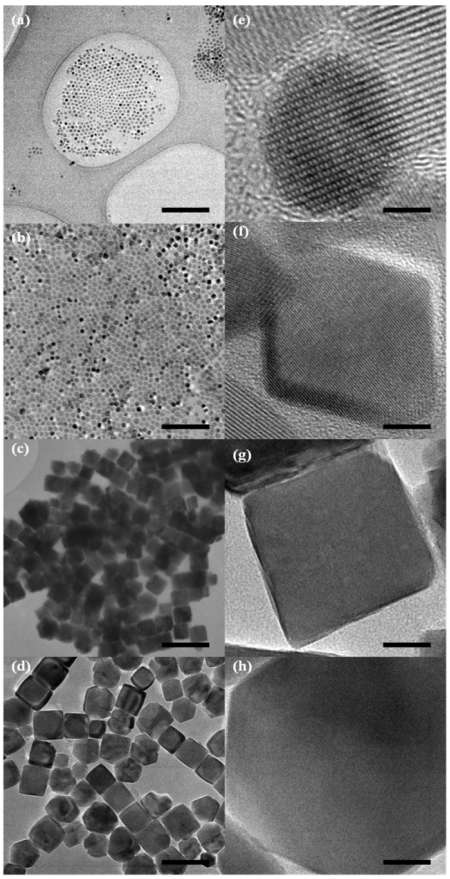

Figure 1. TEM images of iron oxide NPs: (a) R1, (b) R2, (c) R3 and (d) R4. HRTEM images of the same NPs: (e) R1, (f) R2, (g) R3 and (h) R4. Scale bars are as follows. (a)-(d) 150 nm, (e) 2 nm, (f) 4 nm and (g)-(h) 15 nm, respectively.

However, to obtain big NPs or even small ones with acceptable crystalline quality, a certain minimum amount of oleic acid (around to 2 mmol) must be present in the reaction mixture in order to participate in the formation of the intermediate metal-complexes (metal oleates) that in turn regulate the nucleation and growth of the NPs through further decomposition. In addition, oleic acid plays an important role on the final size and dispersity of the particles since it forms a dynamic layer around the nuclei that actively controls the growing process. This was evidenced by synthesizing sample R5 without oleic acid in the reaction mixture. In this way, TEM image in Fig. S3a for sample R5 shows irregular particles in shape with D_{TEM} = 10.6 nm, size much smaller than those obtained with 2-3 mmol of oleic acid. Besides, particles in sample R5 form aggregates as a consequence of poor benzyl-ether coating, and HRTEM images (see Fig. S3b and S3c, Supporting information) reveal the presence of NPs with different grade of crystalline quality that results from a bad control of the particle formation yielding partial coalescence of small crystallites and non-homogeneous particle growing.

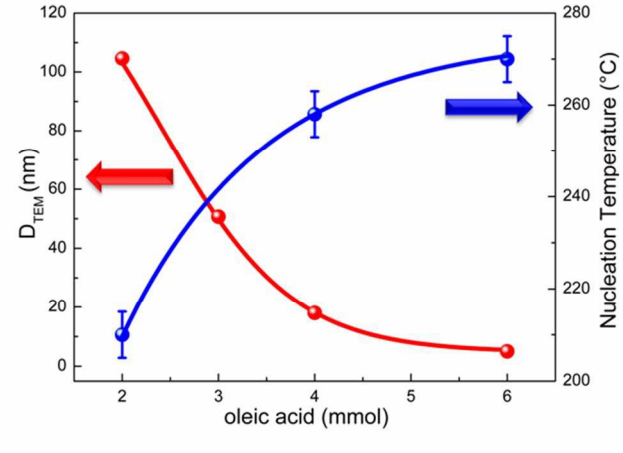

Figure 2. Dependences of the particle size obtained from TEM (red spheres) and the nucleation temperature (blue spheres) as a function of the oleic acid concentration in the reaction mixture. The solid lines are guides to the eye.

Samples R1-R5 were also characterized by XRD diffraction spectroscopy (see Fig. 3 and S3e, Supporting information). All XRD patterns were indexed to a spinel structure without significant traces of any other Fe-oxide compounds. In addition, although there is agreement between D_{TEM} and D_{XRD} for R1 and R2, D_{XRD} is slightly smaller than D_{TEM} for R3-R5 due to the lack of perfect crystallinity of those samples.

TGA spectra for R1-R4 samples show the typical two weight-loss plateaus between 200-400 ºC and 500-750 ºC, that correspond to the removal of both the free oleic acid present in the samples and that attached to the surface of the NPs, respectively.[22] The slight weight-loss below 200 ºC is attributed to the evaporation of adsorbed water molecules.[22] The total weight-loss is within 27% and 3%, where the extreme values correspond to R1 and R4 samples, respectively (see Fig. S4, Supporting information).[22, 24] The reduction in the weight-loss as the size of the particles increases can be explained in terms of the smaller surface to volume ratio for the bigger particles (samples R3 and R4).

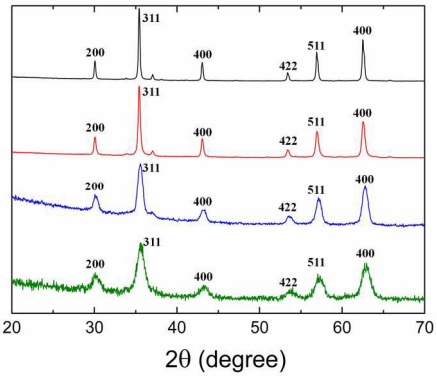

Figure 3. X-ray diffraction patterns together with the indexation of the Bragg peaks to an inverse spinel structure. Samples are showed as follows: R1 (solid green line), R2 (solid blue line), R3 (solid red line) and R4 (black solid line).

Magnetic characterization

First, the magnetic properties of the samples were studied by measuring hysteresis loops at 5 K with a maximum field of ± 50 kOe (see Fig. 4). All curves showed high values of M_s very close to that of bulk magnetite (98 emu/g at 5 K) (see Table 1) and similar to those published elsewhere,[1, 20, 21,23,24] which are associated with an almost perfect bulk-like ferrimagnetic order throughout the whole NPs. In addition, H_c at 5 K rose consistently with particle size from 264 ± 2 up to 327 ± 2 Oe for samples R1 to R3 (see inset to Fig. 4), since particles can be considered as single domain in this range of sizes. The high value of H_c found for R4 may be related to the tendency of those large, faceted particles to pile up forming linear chains (see Fig. 1d).[25] Interestingly, sample R5 showed particle-like behaviour, with a strong reduction of M_s and an increase of H_c in comparison to samples R1-R3 (see Table 1), which is characteristic of crystalline-defective particles.[15]

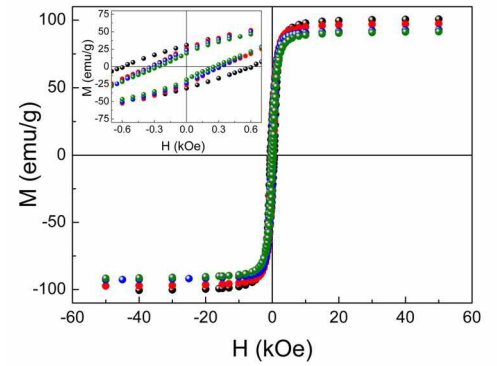

Figure 4. Hysteresis loops at 5 K. Samples are as follows: R1 (green spheres), R2 (blue spheres), R3 (red spheres) and R4 (black spheres). Inset: detail of the low-field region to evaluate the coercive fields.

In order to discard the existence of other magnetic species in the samples, hysteresis loops were recorded at 5 K after cooling the samples under 10 kOe from room temperature (see Fig. 5 and S4, Supporting information). None of the measured loops exhibited the typical features of particles containing ferromagnetic, antiferromagnetic (FeO in wustite phase) and/or ferromagnetic phases in close contact with each other, i.e. shifts along either the magnetic field or magnetization axes – exchange bias effects -.[13,26] Despite this fact, some FC effects on the hysteresis loops are evident in the group of samples R3-R5 in contrast with the invariance of the curves for R1 and R2 after FC. In the cases of R3 and R4, the increase in the magnitude of the magnetization after FC along the whole hysteresis loops could be attributed to a magnetic rearrangement of either some amount of multidomain particles or particle aggregates present in those samples because of their large size or special geometry.[27] On the contrary, the observed slightly effect of FC on the hysteresis loops for sample R5 (see Fig. S5a) could be originated at the enhancement of the magnetic order in NPs where ferrimagnetism is downgraded by crystalline defects.

Finally, the temperature dependence of the magnetic properties was measured. $M_{ZFC} - M_{FC}$ measurements were carried out under a field of 50 Oe and the results for the five samples are shown in Fig. 6 and S5, Supporting Information. $M_{ZFC} - M_{FC}$ curves for sample R1 branch off below about 235 K and M_{ZFC} develops a maximum around 150 K accordingly to the progressive blocking of a distribution of superparamagnetic magnetite NPs of about 7 nm in average size.

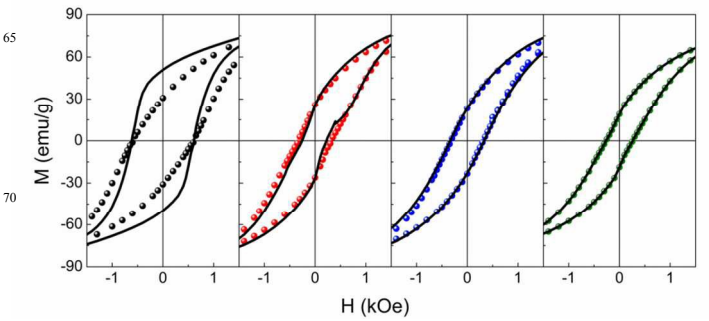

Figure 5. Comparison between the hysteresis loops collected at 5 K before and after FC the sample. Symbols are as follows. R1 (green spheres), R2 (blue spheres), R3 (red spheres) and R4 (black spheres), and the corresponding hysteresis loops of the samples after FC at 10 kOe (solid black lines).

On the contrary, $M_{ZFC} - M_{FC}$ curves for samples R2-R4 exhibit a completely different behaviour: NPs remain blocked even at room temperature as expected for bigger particles. Besides, there is a magnetization jump in the M_{ZFC} curves around $T \approx 120$ K which is attributed to the Verwey transition. Note that this transition is very sensitive to very small changes in the oxygen content of the magnetite phase,[28] so its observation in samples R2-R4 proves their accurate stoichiometry. On the other hand, $M_{ZFC} - M_{FC}$ curves for sample R5 (see Fig. S5b, Supporting information) show some kind of mixing between those two observed behaviours since the mean particle size is in between those for samples R1 and R2 and there might be a coexistence of superparamagnetic and blocked particles even at room temperature.

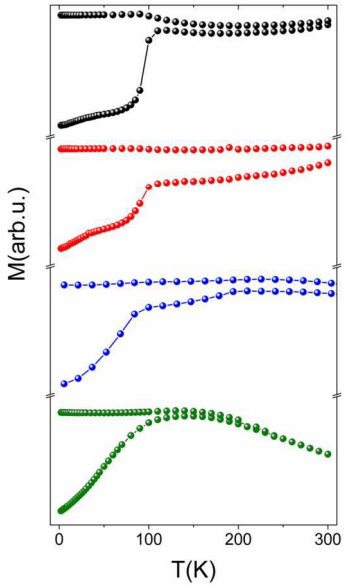

Figure 6. $M_{ZFC} - M_{FC}$ curves as a function of temperature. Samples are as follows: R1 (green spheres), R2 (blue spheres), R3 (red spheres) and R4 (black spheres).

FTIR spectra

So as to study the reaction mechanisms, 4 aliquots (2 mL) of the reaction mixtures collected at different stages of the reactions R1, R2, R4 and R5 were studied by FTIR spectroscopy (see Fig. 7). Figures 7a,b show the spectra of the reactions mixtures at 100 and 200 ºC, respectively. The bands shown in these two spectra are as follows. At long wavelengths (1725-1675 cm^{-1}), two bands appear associated with the stretching modes of the C=O in the COOH group and C=C which correspond to the oleic acid and benzyl-ether molecules, respectively (see the spectra for oleic acid and benzyl-ether in Fig. S6, Supporting Information).[29, 30] In addition, three bands characteristic of aromatic groups (stretching of C=C) are located between 1620-1580 cm^{-1} and 1515-1475 cm^{-1} (see the spectrum of benzyl-ether in Fig. S6, Supporting information). [30] At lower wavelengths, a typical band located at 1525 cm^{-1} and associated with the stretching mode of the C-O group of the $Fe(acac)_3$ is observed (see the spectrum of the $Fe(acac)_3$ in Fig. S6, Supporting information).[31] It is worth noting that the depth of this peak decreases slightly from 100 to 200 ºC (see Fig. 7a,b) suggesting that the $Fe(acac)_3$ starts to decompose below 200 ºC. In addition, the depletion of the peak in this range of temperatures results more abrupt once the amount of oleic acid increases, suggesting that it enhances the decomposition of the $Fe(acac)_3$ and the formation of an intermediate iron complex (Fe^{3+}-oleate).

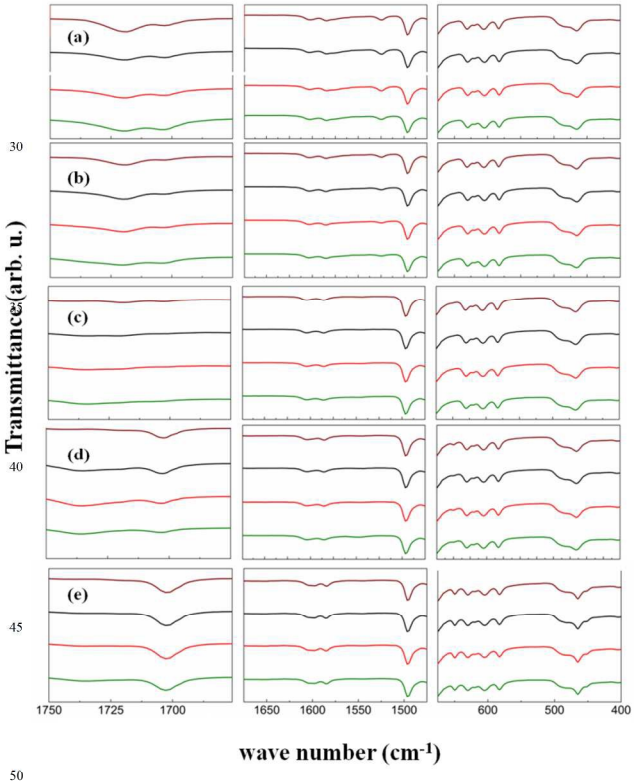

Figure 7. IR spectra for the reaction mixtures at (a) 100 ºC, (b) 200 ºC (0 min), (c) 200 ºC (120 min), (d) 270 ºC (0 min) and (e) 270 ºC (60 min). Curves are as follows: R1 (solid green line), R2 (solid red line), R4 (solid black line) and R5 (solid brown line).

On the other hand, four bands located between 675-400 cm^{-1} are associated with the bending modes of C-H group for the benzyl-ether (see Fig. S6, Supporting information).[30]

After 120 min at 200 ºC, the FTIR spectra of the reaction mixtures shown in Fig. 7c indicated the complete decomposition of $Fe(acac)_3$ (no trace of the peak at 1525 cm^{-1}), and the partial reaction of the benzyl-ether and the oleic acid with the $Fe(acac)_3$ to form Fe^{3+}-complexes since a significant shrinkages of the peaks in between 1725-1675 cm^{-1} were also observed. It is worth noting that the spectra at lower wave numbers (675-400 cm^{-1}) do not show any difference with the spectra at lower temperatures.

When the temperature of the reaction mixtures was risen up to 270 ºC (see Fig. 7d), the spectra for all the samples showed two additional bands between (1720-1685) and (675-630) cm^{-1} that are associated with the stretching modes of C=O and Fe-O groups, respectively. These results indicate the formation of $Fe_{3-x}O_4$ NPs and the attachment of an Fe^{3+}-complex to the NPs' surface. After keeping the reaction mixtures 60 min at this temperature (see Fig. 7e), a dramatically increase of the peaks are observed together with the appearance of a new band between 500-450 cm^{-1} (Fe-O stretching), which in fact is a typical band observed in $Fe_{3-x}O_4$ NPs.[32] From these results one could conclude that both nucleation and growth processes of the NPs take place between 200 and 270 ºC.

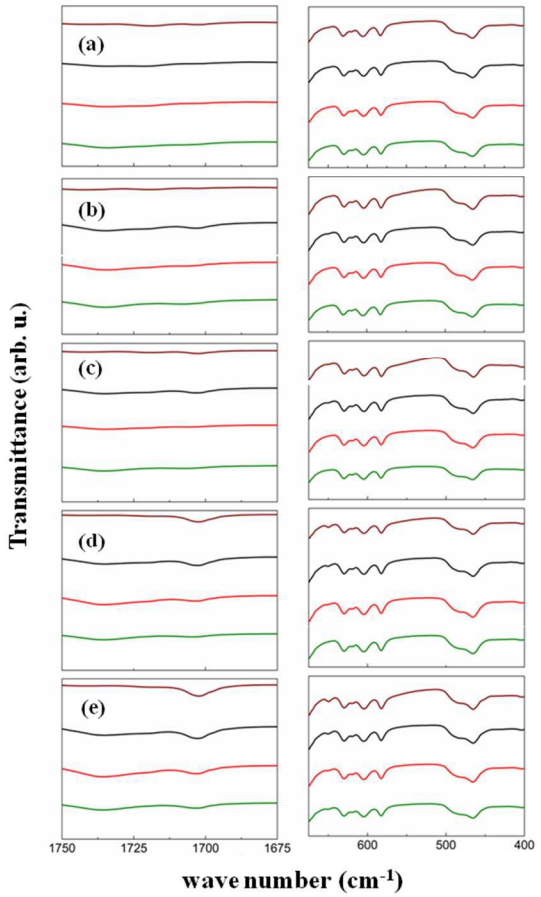

Figure 8. IR spectra for the reaction mixtures between 200 and 270 ºC. (a) 200 ºC, (b) 210 ºC, (c) 230 ºC, (d) 260 ºC and (e) 270 ºC. Curves are as follows: R1 (solid green line), R2 (solid red line), R4 (solid black line) and R5 (solid brown line).

In order to determine the temperatures at which the nucleation and growth processes actually occur, 7 aliquots (1 mL) of the reaction mixtures for samples R1, R2, R4 and R5, taken every 10 º C between 200-270ºC, were studied by FTIR spectroscopy (see Fig. 8 and Fig. S7 and S8, Supporting information). Figure 8 shows the occurrence of a stepped nucleation process depending on the concentration of oleic acid in the reaction mixture. While at 200 ºC (after 120 min) there is no evidence of particles' nucleation for any reaction mixture (see Fig. 8a), the appearance at 210 ºC (see Fig. 8b) of the two new bands between (1720-1685) and (675-630) cm^{-1} for sample R4 (2 mmols of oleic acid) is a clear indication of the onset of the nucleation process for this low concentration of oleic acid. The nucleation temperatures for the reaction mixtures with higher concentration of oleic acid are around 260 ºC for sample R2 (4 mmols of oleic acid) (see Fig. 8d) and 270 ºC for sample R1 (6 mmols of oleic acid) (see Fig. 8e). At the same time, the spectra at 270 ºC (Fig. 8e) show a significant increase in the intensity of those two peaks for samples R2 and R4 indicating that the growth process comes about already between the nucleation and reflux temperatures. These results are summarized in Fig. 2, where the dependences of the nucleation temperature and the mean size of the NPs on the concentration of oleic acid are plotted together. From the comparison of these two curves it can be concluded that the higher the nucleation temperature the smaller the size of the particles, since the temperature interval in which the growth process takes place is progressively reduced as the nucleation temperature increases. Moreover, the nucleation temperature for the reaction without oleic acid (sample R5) is about 230 ºC (see Fig. 8c), however the final size of the particles is much smaller than expected when comparing with the cases of samples with similar nucleation temperatures (R3 and R4) but with oleic acid present in the reaction mixture. This result confirms the greater affinity of the oleic acid as coordinating group for iron than that of the benzyl-ether alone.

Summarizing these analyses, the formation of monodisperse NPs over a wide size is intrinsically related to the separation of the nucleation and growth processes along the reaction as was described by La-Mer and the amount of the surfactant on the reaction mixture.[23,24,33] In the first stages of the reaction, $Fe(acac)_3$ decomposes forming Fe^{3+}-complexes at 200 ºC in a slow process. The onset of the nucleation process takes place at higher temperature while the reaction mixture is heated up to 270 ºC at a constant rate. However, we have observed that the nucleation temperature is strongly dependent on the amount of oleic acid in the reaction mixture. Once the concentration of oleic acid increases, the nucleation temperature rises as well and consequently the growth process can be tuned.[17,33,34] Besides, the concentration of the surfactant self-regulates the growing of the NPs by becoming attached to the particle surface forming a surfactant coating that hinders the aggregation of more nuclei to the particle (see Fig. 9 for a schematic representation of the role of the oleic acid on the final size and shape of the NPs). Interestingly, it is also possible synthesizing NPs with only the presence in the reaction mixture of benzyl-ether acting simultaneously as solvent and surfactant (sample R5). Although the reaction mechanisms involved in this case are pretty similar to those for R1-R4, the obtained particles are much more polydisperse and crystalline defective (see Fig. S3, Supporting information) since benzyl-ether is both a worse surfactant and coordinating group for iron than oleic acid is.[35]

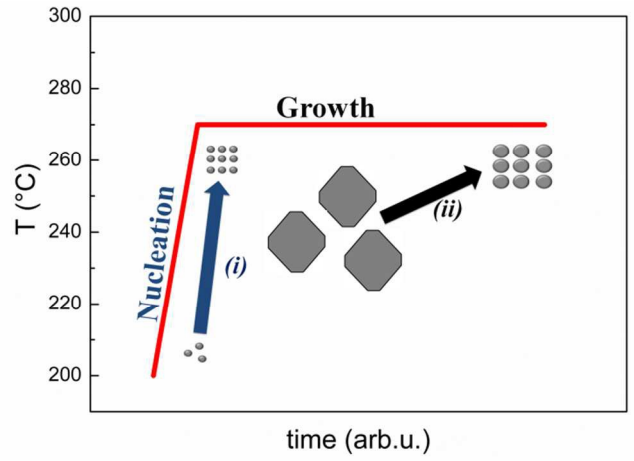

Figure 9. Schematic representation of the role of the oleic acid on the size of the NPs. Arrows at *(i)* and *(ii)* indicate an increase on the concentration of the oleic acid in the reaction mixture and the subsequent effect on the nucleation temperature, and the particle size and shape.

Conclusions

We have shown the effect of the concentration of oleic acid on the synthesis of $Fe_{3-x}O_4$ NPs using benzyl-ether as a solvent. This synthesis method enables the formation of monodisperse NPs ranging from 7 to 100 nm. Structural and magnetic characterization of the samples indicate highly crystalline, single-phase NPs, with values of M_s close to the bulk material and for NPs bigger than 7 nm exhibiting the typical Verwey transition associated with a composition very close to stoichiometric magnetite. In addition, the study by FTIR of the reactions mixtures at various stages contributes to the characterization of the nucleation and growing processes of the NPs. First, $Fe(acac)_3$ decomposes forming an intermediate iron complex at 200 ºC in a slow process. After that and depending on the oleic acid concentration in the reaction mixture, different nucleation temperatures have been observed. Finally, particle growth takes place mainly at the boiling point of the mixture, where the amount of oleic acid plays a self-regulating role on the final particle size by surface coating. Interestingly, the sample synthesized without oleic acid yielded highly defective crystalline NPs of about 10 nm in size, with low values of M_s , in accordance with uncompleted particle formation and poor surfactant coating. All in all, the careful control of the structural and magnetic properties of magnetite nanoparticles is of crucial interest to make them suitable for a number of technological and bio applications.

Acknowledgements

This work was supported by Spanish MINECO (MAT2012-33037), Catalan DURSI (2014SGR220) and European Union FEDER funds (Una manera de hacer Europa).

Notes and references

Departament de Física Fonamental, Institut de Nanociència i Nanotecnologia, Universitat de Barcelona, Martí i Franquès 1, Barcelona 08028, Catalonia, Spain . E-mail: cmoya@ffn.ub.es

Electronic Supplementary Information (ESI) available: For samples R1-R4, particle size distribution and thermogravimetric curves. HRTEM images for samles R3 and R4. For sample R5, TEM and HRTEM images, size distribution, XRD spectrum, hysteresis loop at 5 K and after field cooling the sample under 10 kOe from 300 K down to the final measuring temperature, zero field cooling and field cooling magnetizations as a function of temperature. FTIR spectra for iron (III) acetylacetonate, benzyl-ether and oleic acid. FTIR spectra for the reaction mixtures between 200 and 270 ºC every 10 ºC.

1 B. D. Cullity and C. D. Graham, *Introduction to Magnetic Materials*, 2011.
2 U. Schwertmann and R. M. Cornell, *Iron Oxides in the Laboratory*, 2008.
3 S. Laurent, D. Forge, M. Port, A. Roch, C. Robic, L. Vander Elst and R. N. Muller, *Chem. Rev.*, 2008, **108**, 2064–110.
4 A. Schätz, O. Reiser and W. J. Stark, *Chemistry a European Journal*, 2010, **16**, 8950–67.
5 G. F. Goya, E. Lima, A. D. Arelaro, T. Torres, H. R. Rechenberg, L. Rossi, C. Marquina and M. R. Ibarra, *IEEE Trans. Magn.*, 2008, **44**, 4444–4447.
6 G. Salas, J. Camarero, D. Cabrera, R. Ludwig, I. Hilger, R. Miranda, P. Morales, F. J. Teran and D.- Jena, *J. Phys. Chem. C*, 2014, **118**, 19985
7 J. Chomoucka, J. Drbohlavova, D. Huska, V. Adam, R. Kizek and J. Hubalek, *Pharmacol. Res.*, 2010, **62**, 144–9.
8 C. Sun, J. S. H. Lee and M. Zhang, *Adv. Drug Deliv. Rev.*, 2008, **60**, 1252–65.
9 R. Mejias, S. Pérez-Yagüe, A. G. Roca, N. Perez, A. Villanueva, M. Cañete, S. Manes, J. Ruiz-Cabello, M. Benito, A. Labarta, X. Batlle, S. Veintemillas-Verdaguer, M.P. Morales, D. F. Barber, C. J. Serna, *Nanomedicine*, 2010, **5,** 397.
10 C. Liang, S. Huang, W. Zhao, W. Liu, J. Chen, H. Liu and Y. Tong, *New J. Chem.*, 2015, **39**, 2651–2656.
11 X. Batlle and A. Labarta, *J. Phys. D: Appl. Phys.* 2002, **35**, R15.
12 C. P. Bean and J. D. Livingston, *J. Appl. Phys.*, 1959, **30**, S120.
13 M. Estrader, A. López-Ortega, I. V Golosovsky, S. Estradé, A. G. Roca, G. Salazar-Alvarez, L. López-Conesa, D. Tobia, E. Winkler, J. D. Ardisson, W. A. A. Macedo, A. Morphis, M. Vasilakaki, K. N. Trohidou, A. Gukasov, I. Mirebeau, O. L. Makarova, R. D. Zysler, F. Peiró, M. D. Baró, L. Bergström and J. Nogués, *Nanoscale*, 2015, **7**, 3002–15.
14 C. Moya, M. del P. Morales, X. Batlle and A. Labarta, *Phys. Chem. Chem. Phys.*, 2015, **17**, 13143.
15 C. Moya, G. Salas, M. del P. Morales, X. Batlle and A. Labarta, *J. Mater. Chem. C*, 2015, **3**, 4522–4529.
16 A. G. Roca, R. Costo, A. F. Rebolledo, S. Veintemillas-Verdaguer, P. Tartaj, T. González-Carreño, M. P. Morales and C. J. Serna, *J. Phys. D. Appl. Phys.*, 2009, **42**, 224002.
17 S. Sun and H. Zeng, *J. Am. Chem. Soc.*, 2002, **124**, 8204–8205.
18 S. Sun, H. Zeng, D. B. Robinson, S. Raoux, P. M. Rice, S. X. Wang and G. Li, 2004, **4**, 126–132.
19 J. Park, K. An, Y. Hwang, J.-G. Park, H.-J. Noh, J.-Y. Kim, J.-H. Park, N.-M. Hwang and T. Hyeon, *Nat. Mater.*, 2004, **3**, 891–5.
20 P. Guardia, A. Labarta and X. Batlle, *J. Phys. Chem. C*, 2011, **115**, 390–396.
21 N. Pérez, F. López-Calahorra, A. Labarta and X. Batlle, *Phys. Chem. Chem. Phys.*, 2011, **13**, 19485–9.
22 A. G. Roca, M. P. Morales, K. O'Grady and C. J. Serna, *Nanotechnology*, 2006, **17**, 2783–2788.
23 P. Guardia, J. Pérez-Juste, A. Labarta, X. Batlle and L. M. Liz-Marzán, *Chem. Commun. (Camb).*, 2010, **46**, 6108–10.
24 P. Guardia, N. Pérez, A. Labarta and X. Batlle, *Langmuir*, 2010, **26**, 5843–7.
25 D. Serantes, K. Simeonidis, M. Angelakeris, O. Chubykalo-Fesenko, M. Marciello, M. del P. Morales, D. Baldomir and C. Martinez-Boubeta, *J. Phys. Chem. C*, 2014, **118**, 5927–5934.
26 J. Nogués, J. Sort, V. Langlais, V. Skumryev, S. Suriñach, J. S. Muñoz and M. D. Baró, *Phys. Rep.*, 2005, **422**, 65–117.
27 D. L. Leslie-Pelecky, R. D. Rieke, *Chem. Mater.* 1996, ***8***, 1770.
28 E. J. W. Verwey *Nature*, 1939, **144**, 327.
29 To see the spectrum of the oleic acid: http://pubchem.ncbi.nlm.nih.gov/substance/24278605#section=Source
30 To see the spectrum of the benzyl ether: http://webbook.nist.gov/cgi/cbook.cgi?ID=C538863&Mask=80
31 To see the spectrum of the $Fe(acac)_3$: http://webbook.nist.gov/cgi/cbook.cgi?ID=C14024181&Mask=80
32 A. G. Roca, M. P. Morales, C. J. Serna, *IEEE Trans.Magn,* 2006, **42**, 3025.
33 V. K. LaMer and R. H. Dinegar, J. Am. Chem. Soc., 1950, **72**, 4847.
34 T. Sugimoto; Monodispersed particles. Elsevier: Amsterdam, Holland, 2001
35 J. de la Fuente and V. Grazu, Nanobiotechnology, Volume 4: Inorganic Nanoparticles vs Organic Nanoparticles, 2012.

Table 1. Summary of the structural, microstructural and magnetic parameters of the samples.

Samples	D_{TEM} (nm)	σ	D_{XRD} (nm)	% weight-loss	M_s at 5k (emu/g)	M_s at 300 K (emu/g)	H_c at 5K (Oe)	H_c at 300 K (Oe)
R1	7.4	0.15	7.1 (0.4)	27	90(1)	75(1)	264(2)	SPM*
R2	16.2	0.14	15.4 (1.0)	17	91(1)	82(1)	320(1)	9(2)
R3	50.7	0.20	44.0 (1.5)	7	96(2)	90(2)	327(2)	82(2)
R4	104.6	0.11	94.0 (2.0)	3	99(2)	91(1)	598(10)	94(2)
R5	10.6	0.21	9.0 (0.5)	2	62 (2)	54 (2)	345 (5)	SPM

*SPM stands for superparamagnetic. Numbers in parentheses correspond to the experimental error.